



# A High Quality Image Denoising Technique with Sub Image Block Classification Technique Using Long Short-Term Memory (LSTM) Network Followed By Bayesian Thresholding

S.L. Shabana Sulthana<sup>1\*</sup>, Dr.M. Sucharitha<sup>2</sup>

## Abstract

Medical image analysis relies heavily on picture denoising. Improved perceptual quality of noisy image samples can speed up the diagnostic procedure in many circumstances. Even though medical image denoising is widely used, the current approaches fail to address the wide spectrum of noise in multidisciplinary medical imaging. In this work, new image denoising will be performed by utilizing Bayesian thresholding with LSTM. Here, 5x5 windowing will be applied in the DWT domain to classify the noise effected coefficients. The LSTM will be trained by combining noisy and regular blocks with manually selected label information. The performance will be evaluated using image denoising performance metrics such as 53.25 of PSNR, 0.98 of SSIM, 0.018 of RMSE etc.

1871

**Key Words:** Medical Image Denoising, Bayesian Thresholding, Discrete Wavelet Transform, AlexNet, Deep Learning, Peak Signal to Noise Ratio.

**DOI Number:** 10.14704/nq.2022.20.8.NQ44206

**NeuroQuantology2022;20(8): 1871-1878**

## Introduction

Noise is a visual representation of unwanted data that degrades the quality of the image. As a method that affects the final image, it is referred as such. When exchanging and acquiring images, noise is typically introduced. Image noise distorts the image's contrast range. Images can be affected by a variety of disturbances, such as Gaussian noise produced by regular sources like particle thermal vibration and the distinct nature of radiation from a warm object. Uncontrollable, ever-increasing noise. As a complex phenomenon, back scattered wave presence corrupts picture value by originating from frequent microscopic dispersed reflections that travel over internal organs and makes it extra difficult for the observer to differentiate fine elements of the image in investigative examinations [1].

Nonlocal means and Wiener filters were utilised in the wavelet-based technique for example, as were partial differential equations and empirical mode decomposition. Using Wiener filters to reduce the impact of non-stationary noise on one- and 2-D biomedical signals, as well as on pictures in general, has proven successful [2]. Additive noise, salt and pepper noise, and multiplicative noise are the most common sources of distortion in practise. Each pixel in an image undergoes a tiny change from its original value when subjected to Gaussian noise. To model this form of noise, the Gaussian distribution is a great choice. This is because of the central limit theorem, which asserts that the sum of distinct sounds tends to approach a Gaussian distribution.

**Corresponding author:** S.L. Shabana Sulthana

**Address:** <sup>1\*</sup>Assistant Professor, Dept. of Electronics and Communication Engineering, SHM College of Engineering and Technology, Kollam; <sup>2</sup>Associate Professor, Dept. of Electronics and Communication Engineering, Vellore Institute of Technology, Hyderabad.



The removal of Gaussian noises by conventional linear filters has a detrimental effect on image edge and texture details [3].

Wavelet transforms are used for image denoising as a noise filtering technique. Decomposition into wavelet space and the coefficients of the image are obtained up to a predetermined decomposition level using wavelet denoising is the first step. The obtained coefficients are then subjected to a variety of noise thresholding methods. Handling CLSM images necessitates extreme caution due to the delicate nature of the signal. After that, the inverse transformation is performed with the thresholded coefficients, and the estimated noisy image is reconstructed [4].

Gaussian noise is the most common type of noise that occurs during the acquisition of images. Salt and pepper noise are most commonly seen when images are transmitted through an unencrypted communication filter. As a result, removing image noise is essential if we are to obtain accurate data without compromising the photographs' visual appeal. There are a variety of filters that can be used to reduce visual noise. Some examples include Geometric and Harmonic Mean Filters; Median Filters; Weiner Filters; Midpoint Filters; Max-Min Filters; Alpha-Tiered Mean Filters; Adaptive Filters; Band Pass; Notch; Band Reject Filters, among others [5].

Rest of document follows these guidelines: The techniques for medical picture denoising that have already been described are discussed in Section II. Image denoising is deliberated in Section III. It is in Section IV that the projected approach, comparative study, and analysis are explained and discussed. Section V, on the other hand, focused on the end result.

### Literature Survey

To reduce the amount of noise in OCT images, Zhao Dong et al. suggested a bespoke generative adversarial network (GAN). The ground truth images were created using a speckle modulating optical coherence tomography (SM-OCT). SM-GAN, a neural network model based on 210,000 SM-OCT images, was trained and validated using these pictures. Images of human fingers and a beating fruit fly heart were used to demonstrate the SM-GAN method's performance. Other advanced denoising networks, such as deep learning-based ones, were used to compare the SM-GAN model's results in terms of denoise performance. With the

SM-GAN model provided here, we conclude that speckle noise in OCT pictures and films can be effectively reduced without sacrificing spatial or temporal resolutions [6]

Biomedical image denoising systems that combine Wiener and partial differential equation (PDE) filtering have been proposed by Salim Lahmiri and Mounir Boukadoum. After removing additive Gaussian noise with the local Wiener filter, the PDE filter is used to the resulting filtered picture to further reduce noise while maintaining the edges of the filtered image. The suggested approach outperformed the local Wiener filter and the PDE filter alone in experiments [7].

Many of Salim Lahmiri's image denoising methods for tBEMD include the partial differential equation (PDE), linear complex diffusion process (LCDP), non-linear complex diffusion process (NLCDP), and DWT. Two medical photos and a regular digital image were used in the experiments. Additive Gaussian noise was used to corrupt the original photos in three different levels. tBEMD outperforms the standard BEMD domain by a wide margin in terms of PSNR, as demonstrated in the experiments using PDE, LCDP, NLCDP, and DWT. It has also been found that tBEMD achieves better when the noise level is low than conventional BEMD. To put it another way: When it's high, costs in terms of processing time are the same. [8] The demonstrated efficacy of the proposed method makes it a viable option for clinical use [8].

Undecimated Wavelet Transform (UWT) was proposed by Sai Kumar and his colleagues as a denoising approach, and we tried out the shrinkage task to remove noise. We tested the appropriateness of several wavelet families for denoising therapeutic images using semi-soft and stein thresholding functions together with conventional hard and soft thresholding functions in the shrinkage step. The results showed that the SWT (Stationary Wavelet Transform) denoised image had a better harmony between smoothness and precision than the DWT [9].

Perceptive deep CNNs were designed by Qingsong Yang et al for CT image denoising, which relies on a perceptual loss as the objective function. A deep convolutional neural network's goal function can be a new measure of perceptual similarity. A denoised output's perceptual features are compared to those of the ground truth in a feature space, rather than straight computing MSE for pixel-to-pixel loss. In this way, not only can image noise be reduced, but crucial structural information can be preserved at



the same time. Our tests with a large sum of CT images have yielded promising consequences [10].

### Proposed Method

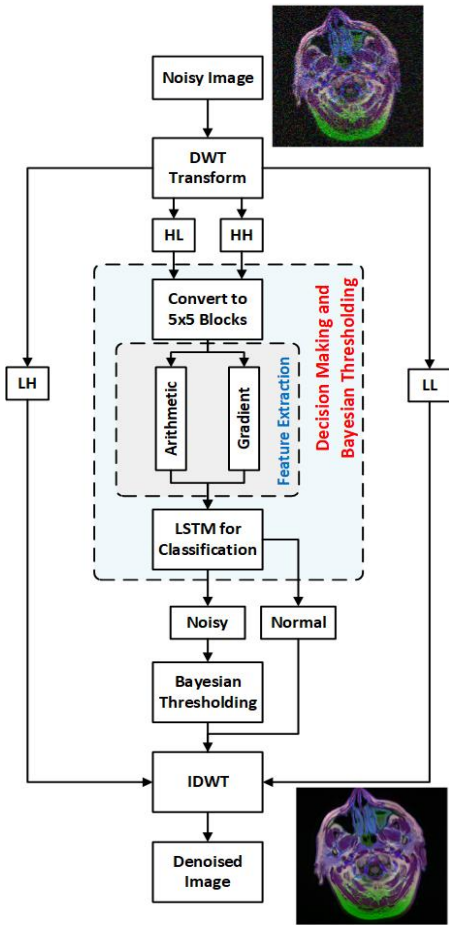


Fig. 1. Block diagram for projected method

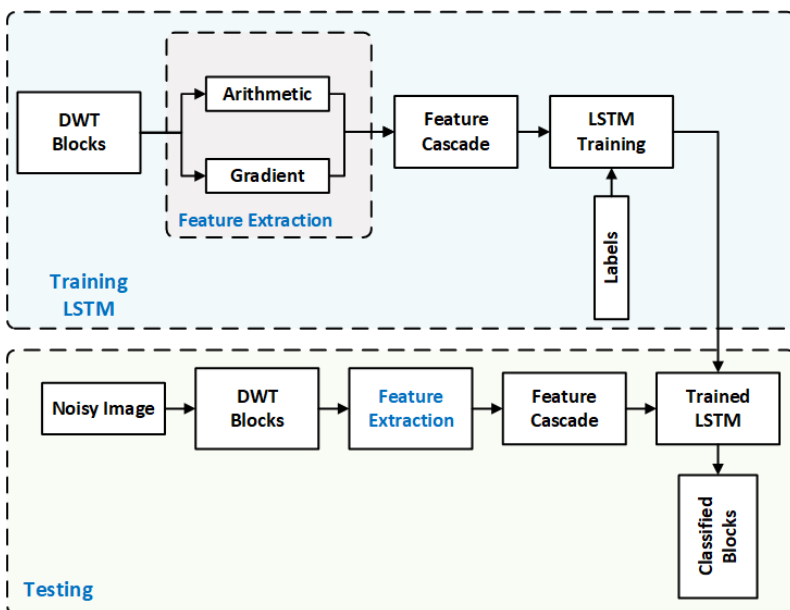


Fig. 2. Training and testing process for DWT block classification



**DWT**

It is better to employ discrete wavelet transforms (DWTs) than Fourier transforms because DWTs have variable window widths and may be scaled. Additionally, DWTs take a lot less computation time than Fourier transforms because they are completed much more quickly. 1-D DWT is used to deconstruct the rows first, and 1-D DWT is used to decompose the columns. LL, HL, HH, and HL are the four decomposed sub-band images that result from this procedure (HH).The LL band from the preceding level is dissected one again by DWT for multi-resolution analysis. As can be seen in Fig. 2, the breakdown levels 1, 2, and 3 are labelled as L (low frequency band) and H. Using a wavelet transformation is preferable because it allows for a changeable window size. Wavelet transform provides a window size that other transforms such as the Fourier and Hilbert transform do not [11].

**Bayesian Thresholding**

An efficient denoising formalism known as Bayesian thresholding was found to be effective. (2) The threshold specified in (1) is best for a white Gaussian noise.

$$T_{\beta}(\sigma_X) = \frac{\sigma^2}{\sigma_X}$$

Where  $\sigma^2$  is the noise variance.

"iid" (independent and identically distributed) noise allows us to write this.

$$\sigma_Y^2 = \sigma_X^2 + \sigma^2,$$

Where  $\sigma_y^2$  is the projected alteration of the experiential image. The projected alteration of signal  $\sigma_x^2$  is then inferred by

$$\sigma_X = \sqrt{\max(\sigma_Y^2 - \sigma^2, 0)}.$$

A robust estimator of the noise alteration is increased by

$$\sigma = \frac{M}{0.6745},$$

where M is the median value of the total wavelet coefficients in the 1<sup>st</sup>.

Assuming that the wavelet coefficients have a Generalized Gaussian Distribution, this threshold setting was shown to be best (GGD). The GGD is influenced by a parameter referred to as the shape factor. Subbands of natural images can be modelled with a value in the 0.5 and 1 range. This value is always set to 1 to make things easier when using the Bayesian threshold. It has been suggested that

this shape factor be included in the computation of the cutoff value.

**Gradient Feature Extraction**

The gradient map can be decomposed into its directional components in this approach. Directly feeding a classifier a gradient map does not produce promising detection results since the gradient map's directionality is not explicitly measured. Using directional gradient features in face detection was inspired by preceding work on on-line character recognition that claimed promising consequences. feature reduction are the three stages necessary to acquire gradient direction features.

**Arithmetic Feature Extraction**

**1. Standard Deviation**

Standard deviation is a measure of the variance of the distribution of a given number, and it is used in statistical analysis. It is easier to establish means when standard deviation is low, whereas it is more difficult to establish a consensus when standard deviation is high. The sample typical deviation is calculated using this formula.

1874

$$s = \sqrt{\frac{1}{N-1} \sum_{i=1}^N (x_i - \bar{x})^2}$$

where  $\{x_1, x_2, \dots, x_n\}$  are the observed values of the sample items,  $\bar{x}$  is the mean value of these comments, N is the sum of observations of the trial.

**Mean**

In statistical terms, the mean is the sum of all observed data divided by the total number of observed data points. It is common to use the symbol to represent the arithmetic mean of an array of numbers (x,) In the sample, there are n items.

$$\bar{x} = \frac{1}{n} \left( \sum_{i=1}^n x_i \right) = \frac{x_1 + x_2 + \dots + x_n}{n}$$

**Kurtosis**

The "tailedness" of a real-valued random variable's probability distribution is assessed by its kurtosis in probability theory and statistics. The four standard points on a graph can be used to plot it:



$$\begin{aligned} \text{Kurtosis}[X] &= E \left[ \left( \frac{X - \mu}{\sigma} \right)^4 \right] = \frac{E[(X - \mu)^4]}{(E[(X - \mu)^2])^2} \\ &= \frac{\mu_4}{\sigma^4} \end{aligned}$$

where  $\mu_4$  is the fourth central instant and  $\sigma$  is the standard deviation.  $K$  signifies the kurtosis.

### Skewness

In probability theory and statistics, skewness is a measure of the asymmetry of the probability distribution of a real-valued random variable relative to its mean. The skewness value can be positive, zero, negative, or undefined.

The skewness of variable  $X$  is the third standardized moment  $\tilde{\mu}_3$  defined as:

$$\begin{aligned} \tilde{\mu}_3 &= E \left[ \left( \frac{X - \mu}{\sigma} \right)^3 \right] = \frac{\mu_3}{\sigma^3} = \frac{E[(X - \mu)^3]}{(E[(X - \mu)^2])^{3/2}} \\ &= \frac{k_3}{k_2^{3/2}} \end{aligned}$$

There are three central moments ( $\mu_3$ ,  $\mu_2$ , and mean) and three cumulants ( $\kappa_3$ ,  $\kappa_2$ , and mean). Skewness is expressed by the ratio of the third cumulant  $\kappa_3$  to the 1.5th power of the second cumulant  $\kappa_2$ .

### Moment

The whole mass is represented by the zeroth moment, the centre of mass is represented by the first moment, and the rotational inertia is represented by the second moment, if the function signifies mass. The zeroth moment of a function that expresses energy is the whole energy. The zeroth moment of a probability distribution is the whole probability (one), and the first moment is the expected value.

Assume that  $f(x)$  is an unbounded real-valued continuous function with respect to some constant

$$\mu_n = \int_{-\infty}^{\infty} (x - c)^n f(x) dx$$

### LSTM

Long-range dependencies in one-dimensional data can be captured using the LSTM network, which is well-known for this purpose. Additionally, it is feasible to use the LSTM network to capture some correlations in multi-dimensional data that require more computation. Multidimensional data can be converted into lengthy, one-dimensional data to achieve this objective. Sparse noise characteristics are extracted using the LSTM network in this section. We must convert the two-dimensional

feature map into a one-dimensional signal in order to get the optimum results. Raster scanning is one scanning format that works well for this. Gradient loss and excessive computational complexity may be encountered when training LSTM networks to deal with extensive one-dimensional input data. To deal with these problems, we suggest a multi-directional LSTM network. When using the LSTM network, inputs are received from all four directions:

Starting from the bottom up (direction 4). There is a risk that our suggested approach will not be able to capture all the noise features because we presume that the LSTM network can only be applied to four directions. A convolutional neural network will first convolutionalize the feature maps before passing them to the directional LSTM module in each direction. In this case, 32 filters are used. To make things easier, the LSTM network will be rotated by  $90^\circ$ ,  $180^\circ$ , and  $270^\circ$  to represent the directions. The LSTM can only be applied from the top to the bottom after rotations. As a result, we should have fewer problems putting this plan into action. A convolutional neural network, 1164, will then process all four directions of input data to produce the feature maps of a multi-directional LSTM network's output feature maps.

## Results and Discussions

### PSNR

It is the ratio of the signal's maximal potential strength to the power of corrupted input [12]. The equation for PSNR is as follows: (8).

$$PSNR = 20 \cdot \log_{10} MAX_{PY} - 10 \cdot \log_{10} MSE \quad (8)$$

$MAX_{PY}$  is the maximum picture pixel value, as seen in the figure.

The unencrypted and encrypted images are denoted by  $K$  and  $k$ , respectively.

### Mean Square Error (MSE)

Estimator consistency can be measured using the MSE; this metric is frequently non-negative, with values around zero being higher [13]. The difference between the encrypted and unencrypted photos is shown in equation by MSE (11).

$$MSE = \frac{1}{P_x * P_x} \sum_{i=1}^{P_x} \sum_{j=1}^{P_x} | \hat{I}(i, j) - I(i, j) |^2 \quad (11)$$

### Root-Mean-Square Error (RMSE)

The standard deviation of the residuals is calculated using the RMSE. Data points are



measured in terms of residuals, a statistic that indicates how far apart they are from the regression line [14]. (12).

$$RMSE = \sqrt{E - K} \quad (12)$$

Where E is the value and K are known results.

**Mean Absolute Error (MAE)**

Errors in matched data that represent the same phenomenon are assessed using MAE (mean absolute error) statistics [15]. It is possible to do a comparison between one measuring technique and another as described in Equation 1 by comparing the projected and observed future times (13).

$$MAE = \frac{\sum_{l=1}^N |Y_l - X_l|}{N} \quad (13)$$

**Natural Image Quality Evaluator (NIQE)**

Even though an NIQE ideal is trained on a pristine image database with arbitrary distortion, NIQE can calculate image quality. The NIQE is unaffected by opinion but does not employ arbitrary quality ratings [16].

**Blind/Reference Less Image Spatial Quality Evaluator**

Visually impaired/non-referenced In order to evaluate the quality of distorted images, the Spatial Quality Estimator (BRISQUE) relies on images that have been previously warped. As a result of this,

BRISQUE photos come with a subjective commentary [17].

**Table I.**Performance Value for the different Density of Noise Medical Images

NoiseLevel	PSNR	MSE	RMS E	MAE	NIQE	BRISQUE
0.01	43.25	78.54	12.48	88.14	4.9	58.24
0.02	42.85	76.15	12.69	84.46	4.82	56.14
0.03	42.19	75.53	13.74	82.17	3.73	55.75
0.04	41.92	73.12	14.25	80.12	3.14	54.96
0.05	41.21	72.19	14.87	79.43	2.79	53.14
0.06	40.55	71.54	15.62	78.41	2.13	53.01
0.07	39.82	70.34	15.87	78.30	2.02	52.43
0.08	37.46	69.40	16.98	77.79	1.98	52.16
0.09	36.57	59.73	17.56	77.12	1.71	51.46
0.10	34.23	58.34	17.81	76.74	1.04	50.14

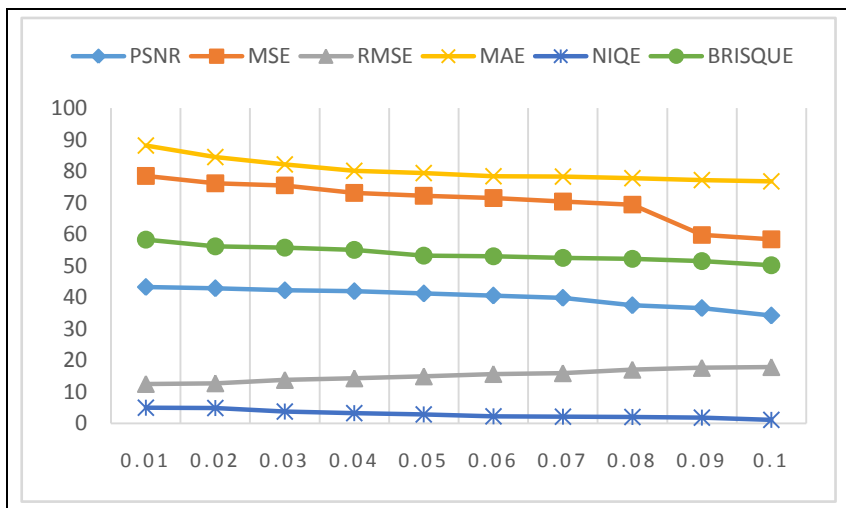


**Fig.3.** Performance of different density of noisy medical image

**Table II.**Comparison of Performance with the Previous Technique

METHOD	SSIM	PSNR	RMSE
GSO [13]	0.92	50.8	1.235
KGMO [14]	0.82	16.1	0.023
Proposed Method	0.98	53.25	0.018



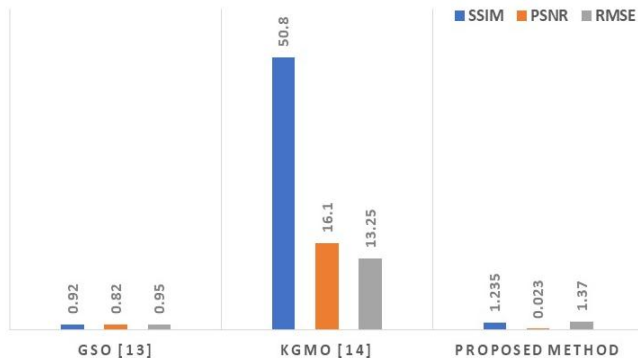


Fig. 4. Comparative performance of proposed method

## Conclusion

LSTM and Bayesian Thresholding are used in this paper to denoise images. It aims to eliminate the Gaussian white noise that can be seen in noisy photos by applying this technique. As a result, a line or curve singularity can be better preserved in noisy images by using the method provided in this study. Image denoising relies heavily on this. The wavelet transform yields the DWT transformation. After converting the image into 5x5 blocks, the algorithm extracts the noisy image's arithmetic and gradient properties. Images can be classified as either normal or noisy using the LSTM algorithm. To reduce the amount of noise in the image, we employ Bayesian Thresholding and IDWT. When compared to prior works, this one performs better. It has an SSIM of 0.98, a PSNR of 53.25, and an RMSE of 0.018.

## References

Laves, Max-Heinrich, Malte Tölle, and Tobias Sa. "Uncertainty estimation in medical image denoising with bayesian deep image prior." In *Uncertainty for Safe Utilization of Machine Learning in Medical Imaging, and Graphs in Biomedical Image Analysis*, pp. 81-96. Springer, Cham, 2020.

Bansal, Mohit, Munesh Devi, Neha Jain, and Chinu Kukreja. "A proposed approach for biomedical image denoising using PCA\_NLM." *International Journal of Bio-Science and Bio-Technology* 6, no. 6 (2014): 13-20.

Thanh, D.N.H., and S.D. Dvoenko. "A denoising of biomedical images." *The International Archives of Photogrammetry, Remote Sensing and Spatial Information Sciences* 40, no. 5 (2015): 73.

Bharati, Subrato, Tanvir Zaman Khan, Prajoy Podder, and Nguyen Quoc Hung. "A comparative analysis of image denoising problem: noise models, denoising filters and applications." In *Cognitive Internet of Medical Things for Smart Healthcare*, pp. 49-66. Springer, Cham, 2021.

Gökdağ, Yunus Engin, Firat Şansal, and Y. Dağhan Gökdel. "Image denoising using 2-D wavelet algorithm for Gaussian-corrupted confocal microscopy images." *Biomedical Signal Processing and Control* 54 (2019): 101594.

Dong, Zhao, Guoyan Liu, Guangming Ni, Jason Jerwick, Lian Duan, and Chao Zhou. "Optical coherence tomography image denoising using a generative adversarial network with speckle modulation." *Journal of biophotonics* 13, no. 4 (2020): e201960135.

Lahmiri, Salim, and Mounir Boukadoum. "Hybrid Wiener and partial differential equations filter for biomedical image denoising." In *2016 14th IEEE International New Circuits and Systems Conference (NEWCAS)*, pp. 1-4. IEEE, 2016.

Lahmiri, Salim. "Image denoising in bidimensional empirical mode decomposition domain: the role of Student's probability distribution function." *Healthcare technology letters* 3, no. 1 (2015): 67-71.

Kumar, K. Sai, K. Nikhil Naga Sai Ram, K. Kiranmai, and S. Sri Harsha. "Denoising of Iris image using stationary wavelet transform." In *2018 Second International Conference on Inventive Communication and Computational Technologies (ICICCT)*, pp. 1232-1237. IEEE, 2018.

Yang, Qingsong, Pingkun Yan, Mannudeep K. Kalra, and Ge Wang. "CT image denoising with perceptive deep neural networks." *arXiv preprint arXiv:1702.07019* (2017).

Yadav, Ashwani Kumar, R. Roy, Archek Parveen Kumar, Ch Sandesh Kumar, and Shailendra Kr Dhakad. "De-noising of ultrasound image using discrete wavelet transform by symlet wavelet and filters." In *2015 International Conference on Advances in Computing, Communications and Informatics (ICACCI)*, pp. 1204-1208. IEEE, 2015.

Nayak, Janmenjoy, Bighnaraj Naik, Paidi Dinesh, Kanithi Vakula, and Pandit Byomakesha Dash. "Firefly Algorithm in Biomedical and Health Care: Advances, Issues and Challenges." *SN Computer Science* 1, no. 6 (2020): 1-36.

Sulthana, SL Shabana. "Highly Efficient Speckle Noise Removal in Medical Images Using GSO Optimization." In *2021 7th International Conference on Advanced Computing and Communication Systems (ICACCS)*, vol. 1, pp. 1368-1373. IEEE, 2021.

Shabana Sulthana S L and Sucharitha. M. "Kinetic Gas Molecule Optimization (KGMO) Based Speckle Noise Reduction in Ultrasound Images". *Soft Computing and Signal Processing (ICSCSP-2020)*, 3rd International conference, 2020.

Subashini, Parthasarathy, Marimuthu Krishnaveni, Bernadetta Kwintiana Ane, and Dieter Roller. "Wavelet based image denoising using ant colony optimization technique for identifying ice classes in SAR imagery." In *Soft Computing Models in Industrial and Environmental Applications*, pp. 399-407. Springer, Berlin, Heidelberg, 2013.

Jia, Lina, Quan Zhang, Yu Shang, Yanling Wang, Yi Liu, Na Wang, Zhiguo Gui, and Guanru Yang. "Denoising for low-dose CT image by discriminative weighted nuclear norm minimization." *IEEE Access* 6 (2018): 46179-46193. DOI: 10.1109/access.2018.2862403

Anoop, Vylala, and Plakkottu Radhakrishnan Bipin. "Medical Image Enhancement by a Bilateral Filter Using Optimization Technique." *Journal of Medical Systems* 43, no. 8 (2019):240.

Yamini P. Chaudhari, Dr. P.M. Mahajan, "Image Denoising of Various Images using Wavelet Transform and Thresholding Techniques" in, *IRJET*, 2017.

Lee, Chang-Ock, Kiwan Jeon, Seonmin Ahn, Hyung Joong Kim, and Eung Je Woo. "Ramp preserving denoising for conductivity image reconstruction in magnetic resonance

electrical impedance tomography." IEEE transactions on biomedical engineering 58, no. 7 2011): 2038-2050.  
DOI: 10.1109/TBME.2011.2136434.

Jia, Lina, Quan Zhang, Yu Shang, Yanling Wang, Yi Liu, Na Wang, Zhiguo Gui, and Guanru Yang. "Denoising for low-dose CT image by discriminative weighted nuclear norm minimization." IEEE Access 6 (2018): 46179-46193.  
DOI: 10.1109/access.2018.2862403

